ACS APPLIED MATERIALS & INTERFACES

Letter

www.acsami.org

Thin Films of Two Functional Oxides Patterned Laterally by Soft Lithography

Ole F. Göbel,[†] Tomasz M. Stawski, and Johan E. ten Elshof*

MESA+ Institute for Nanotechnology, University of Twente, P.O. Box 217, 7500 AE Enschede, The Netherlands

ABSTRACT: Thin films of two laterally patterned functional oxides of uniform thickness were obtained in a two-step soft-lithographic micromolding process. $CoFe_2O_4$/ZnO and $CoFe_2O_4$/$BaTiO_3$ dual-phase patterns were fabricated. The films showed good replication of the pattern that was defined in the first patterning step. X-ray diffraction showed that the films consisted of two distinct phases, and magnetic force microscopy showed that the compounds were laterally separated, the separation pattern being the same as that of the initial soft-lithographic process. The films exhibited slight height variations near the edges of the phases, which were introduced in the first deposition step and were not fully compensated in the second deposition step. The films are sufficiently smooth to allow fabrication of multilayer structures.

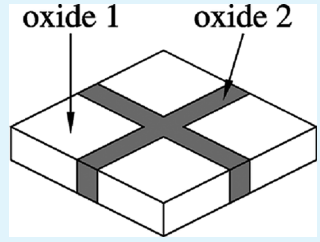

KEYWORDS: *micromolding, soft-lithography, oxides, micropatterning, sol–gel*

1. INTRODUCTION

Soft-lithographic patterning[1] of functional oxide films is regarded as a cost-effective and versatile method to pattern relatively large areas with micrometer-scale to nanometer-scale resolution, e.g., refs 2–4 and references therein. Soft-lithographic techniques include methods such as micromolding, micromolding in capillaries, microtransfer molding, and capillary force lithography.[4] Oxide materials patterned by one of these means include perovskites, spinels, high T_c superconductors, and binary oxides such as ZnO and TiO_2. Lateral resolutions below 200 nm have been demonstrated for oxides,[5,6] and below 50 nm for UV-curable siloxanes.[7] In nearly all published cases, the soft-lithographic patterning is restricted to one material and films have a pronounced relief, which may not be very suitable for the deposition of one or more additional layers. We recently showed that stacks of up to 6 layers of arbitrarily oriented oxide line patterns could be printed directly over each other by micromolding sol–gel precursors.[8] A larger number of layers was not possible because of the increasingly uneven topography of the substrate, which the flexible PDMS mold was no longer able to follow without leakage. In the present work, we demonstrate an approach to make thin films consisting of two different, laterally patterned oxides, which cover the surface of the substrate side by side. Apart from being useful as such, such microstructured films have a homogeneous thickness and could also serve as substrates for subsequent deposition of further oxide layers, this allowing a true bottom-up approach for the fabrication of 3D micro- or nanoscale devices. We chose $CoFe_2O_4$/$BaTiO_3$ and $CoFe_2O_4$/ZnO as examples to demonstrate the versatility of our method, but the method is also applicable to a large number of other materials.

2. EXPERIMENTAL SECTION

$CoFe_2O_4$ and ZnO were grown from polymeric precursor solutions. The ZnO precursor was prepared as described in ref 8. The $CoFe_2O_4$ precursor solution was prepared by dissolving 560 mg of $Co(NO_3)_2{\cdot}6H_2O$ (Fluka), 1210 mg of $Fe(NO_3)_3{\cdot}9H_2O$ (Merck), and 1.77 g of poly(acrylic acid) (M_w = 1800 g/mol, Aldrich) into a mixture of 1.77 g of water and 1.78 g of 2-methoxyethanol.

$BaTiO_3$ was obtained from a sol–gel precursor prepared as described elsewhere.[9] The concentration of the barium titanate precursor solution was 0.5 mol/dm^3, and the hydrolysis ratio was 2.8. Substrates used were (001)-cut Si wafers with a native oxide layer or a grown SiO_2 layer of several 100 nm thickness. Prior to the first deposition, the substrates were cleaned by snow-jetting and oxygen plasma cleaning.[8,10] Molds were prepared from poly(dimethylsiloxane), PDMS (Sylgard 184, Dow Corning) as described elsewhere.[8] The depth of the relief patterned molds was 2 μm in all experiments, and the dimension of the molds was 1 × 1 cm^2. The deposition of the second precursor was carried out with a flat PDMS slab obtained by casting the liquid PDMS against a flat silanized Si wafer, but otherwise following exactly the procedure for patterned molds. The patterning process and accompanying conditions are described in the Results and Discussion section.

Patterned samples were analyzed after each step of preparation by several methods: a) optical microscopy with a Nikon Eclipse 990 ME; b) atomic force microscopy (AFM) with a Bruker Dimension Icon, a Bruker Multimode 8, and a Bruker Dimension 3100, operated both in contact mode and tapping mode; (c) high-resolution scanning electron microscopy (HR-SEM) with a Zeiss 1550, and (d) X-ray diffraction with a Philips PW 3020 powder diffractometer with monochromated Cu Kα radiation. The topography of the calcined samples was measured in tapping mode, simultaneously with the magnetic field (magnetic field microscopy, MFM). For these combined AFM/MFM scans the samples were placed in the magnetic field of a permanent Nd–Fe magnet for 24 h prior to scanning. The Fe/Co-coated AFM tips were magnetized for a few minutes prior to scanning. It can be assumed that this treatment yields samples and AFM tip with saturated magnetization.

Received: October 25, 2011
Accepted: December 12, 2011
Published: December 12, 2011

   dx.doi.org/10.1021/am201474t | *ACS Appl. Mater. Interfaces* 2012, 4, 40–43

3. RESULTS AND DISCUSSION

The patterning process was carried out in two deposition steps, which are illustrated schematically in Figure 1a–d. Patterning

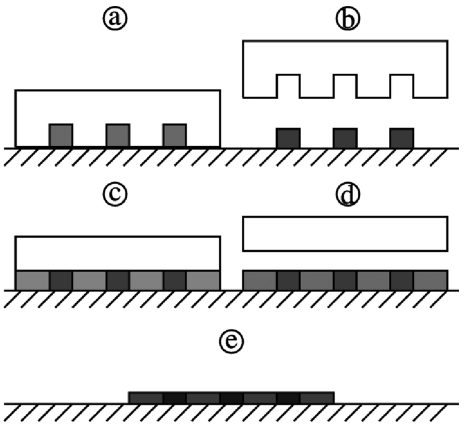

Figure 1. Micromolding process. (a) First step: patterned mold (white) on substrate, confining precursor #1 (gray); (b) after first step: mold removed, exposing dried solid precursor #1; (c) second step: flat PDMS slab engaged on patterned precursor #1 film (dark gray), confining precursor #2 (light gray); (d) after second step: removed PDMS slab, exposing laterally patterned film of precursors #1 and #2; (e) after heat treatment: shrunk, laterally patterned film of oxides #1 and #2.

was followed by pyrolysis/sintering (Figure 1e). In the first step, a droplet of a few μL of $CoFe_2O_4$ precursor solution, sufficient to fil all the receding features of the mold, was placed on the substrate and heated to 30 °C. The mold was pressed into the droplet with a pressure between 1.2 and 1.5 bar at the contact interface substrate/PDMS. Immediately thereafter, the sample was heated to 80 °C with the mold still adhered to the substrate. The process is essentially similar to the procedure outlined in ref 10, thus preventing formation of a residual layer between the patterned features. After ~30 min, when the precursor solution had solidified sufficiently by diffusion of solvent into PDMS, the mold was removed. The sample was then heated to 200 °C with a rate of 10 °C/min and held at this temperature for at least 1 h, thus ensuring that the patterned precursor film was totally dry and stable for several days at least.

Figure 2 depicts optical and atomic force microscope (AFM) images of two $CoFe_2O_4$ samples. Two height profiles at the bottom of Figure 2 were derived from the corresponding AFM images above, in which the locations of the profile are indicated by the white dotted lines. The films show considerable height variations near the edges of the features. Similar double-peak topographies were first reported by Martin and Aksay on sol–gel derived lead zirconate titanate (PZT) patterns by micromolding in capillaries (MIMIC),[11] but they have also been reported for other materials after micromolding.[8,10] The double peak topography prior to thermal treatment was rather pronounced for the dried $CoFe_2O_4$ precursor pattern. Figure 2 shows central planar regions of ~200 nm thickness, and edge regions with a thickness of 350–450 nm. These dried $CoFe_2O_4$ precursor micropatterns presented a good case to investigate to what extent height variations in the first pattern after drying at 200 °C evolve in the course of the second step of the patterning process and afterward during thermal treatment.

The deposition of the second precursor solution, i.e., for $BaTiO_3$ and ZnO, was done in practically the same manner, the

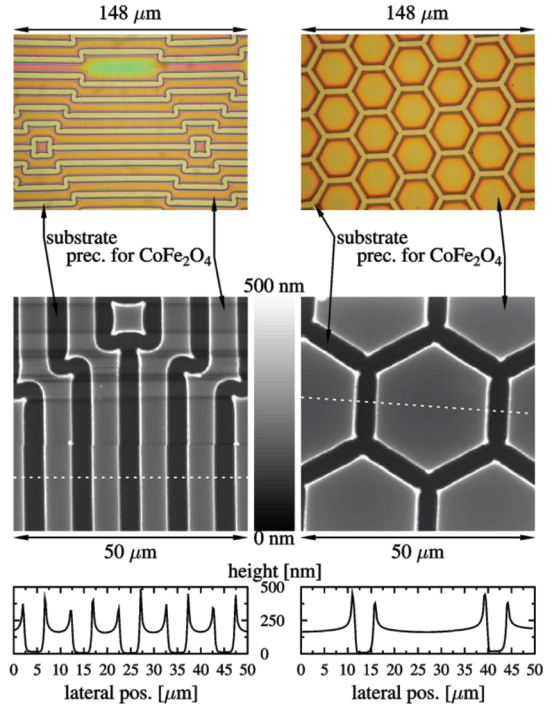

Figure 2. Optical microscope images (top row), AFM images (middle row), and height profiles (bottom row) of two samples after the first deposition step and subsequent drying.

only difference being the use of a flat PDMS mold instead of a patterned mold to press the second precursor solution onto the film of the first precursor with a pressure of 1.2–1.5 bar. Optical microscope and AFM images of the two samples of Figure 2 after deposition and drying of the second precursor are shown in Figure 3. It can be seen that the edge height of both $CoFe_2O_4$ precursor patterns was lower than before the deposition step, which indicates that the patterns were flattened by the second molding step with a flat PDMS stamp. The absolute thickness of the dual-phase films was determined by making a scratch through the film onto the substrate and scanning through this scratch with the AFM (scans not shown). In this manner, the thickness of the $CoFe_2O_4/BaTiO_3$ films was determined to be ~170 nm, and the thickness of the $CoFe_2O_4$/ZnO films was 240 nm. These numbers have to be compared with the thickness of the patterned films after $CoFe_2O_4$ deposition step and drying, which was ca. 160 nm for both films.

We can conclude that the $BaTiO_3$ precursor added only little to the total film thickness, i.e. the thickness of the elevated parts. Obviously, the amount of $BaTiO_3$ precursor material deposited on top of the $CoFe_2O_4$ precursor was small, and/or its shrinkage during drying was high. Both assumptions are reasonable. The sol–gel $BaTiO_3$ precursor has a relatively low viscosity η = 4.5 mPa.s at 20 °C, and can thus be pressed away sideways easily.[5] The solution also has a low concentration of only 0.5 mol/dm^3. This will result in large shrinkage upon drying and thermal treatment. On the other hand, the deposition of the ZnO precursor solution on the dried $CoFe_2O_4$ precursor pattern increased the total film thickness substantially, which can be explained by the large amount of ZnO precursor deposited on top of the $CoFe_2O_4$ precursor, and/or its relatively low shrinkage upon drying. Both explanations are probably valid, since the viscosity and

dx.doi.org/10.1021/am201474t | ACS Appl. Mater. Interfaces 2012, 4, 40–43

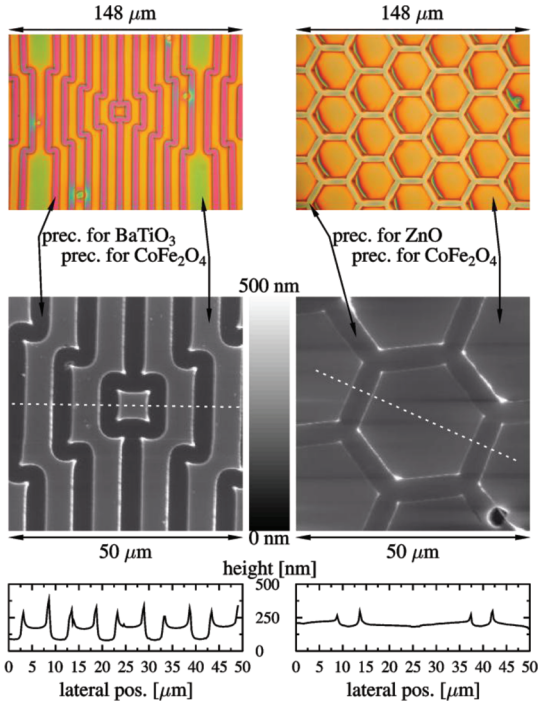

Figure 3. Optical microscope images (top row), AFM images (middle row), and height profiles (bottom row) of two samples after the second deposition step and subsequent drying. The abolute film thicknesses were ca. 170 and 240 nm, respectively.

concentration of the polymer-based ZnO precursor are high, i.e., η = 47 mPa s, and $[Zn^{2+}]$ = 1.10 mol/dm^3, respectively. The dried $CoFe_2O_4$/ZnO and $CoFe_2O_4$/$BaTiO_3$ precursor films were stable for weeks before the final pyrolysis-crystallization-sintering step was applied. For this purpose, the samples were heated with 10 °C/min to 300 °C, and then with 5 °C/min to 400 °C and held at this temperature for 1 h to ensure extensive decomposition of the precursors without simultaneous initiation of crystal growth. They were further heated with 10 °C/min to 800 °C and held at this temperature for another hour before cooling to room temperature with −10 °C/min or slower.

The resulting samples are depicted in Figure 4. The films clearly show laterally distinct regions with different phases, and good replication of the pattern defined by the first molding step. The films also exhibit a residual topography with height variations of ∼100 nm over lateral distances of ∼2 μm. This suggests that multiple layer patterning is possible with this method. But since the substrate roughness will increase with each additional layer, the maximum number of layers that can be added will probably be limited to ∼10 or less.[8] The height differences were mainly introduced in the first deposition step and were not fully compensated in the second deposition step, nor in the subsequent drying and calcination steps. To obtain flatter precursor films after the second deposition step or after the final heat treatment, it appears necessary to tune the concentration and viscosity of the second precursor solution. The concentration is easy to control by modifying the recipe of its synthesis. The viscosity can be adjusted via the recipe and/or the temperature at which the precursor is deposited.

A similar soft imprinting technique has been used to fabricate a woodpile structure of silica, by patterning a very concentrated (88 wt %) predried methylsilsesquioxane-silica sol−gel silica precursor, followed by planarizing the layer using polystyrene.[12]

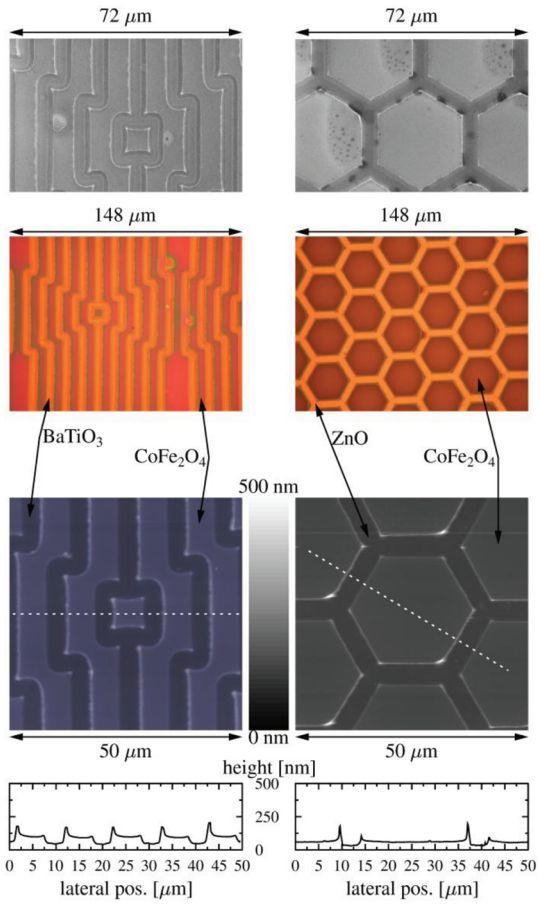

Figure 4. SEM images (top row), optical microscope images (second row), AFM images (third row) and height profiles (bottom row) of two samples after thermal treatment. The abolute film thicknesses of the elevated areas were determined in additional AFM scans across scratches through the films as ca. 100 and 60 nm, respectively.

Residual layers (∼15 nm thick) after imprinting were removed with a short acid etch. The high solids content of the precursor ensured minimal shrinkage (∼7%) and good shape replication. Unfortunately, metal oxide precursors cannot be concentrated to such an extent, so that considerable shrinkage and/or the occurrence of double peak topographies are much harder to avoid.

The MFM images in Figure 5 show a clear contrast in phase lag between the two types of domains, i.e. between the higher ones, derived from the $CoFe_2O_4$ precursor and the lower ones, derived from the $BaTiO_3$ and ZnO precursors, respectively. This finding proves that the domains have different degrees of remnant magnetization, and thus they are made of different materials. The conclusion is supported by the X-ray diffractograms in Figure 5, middle and bottom, of the two samples. Though the peaks are weak in general and those of $CoFe_2O_4$ in particular, the diffractograms expose the strongest peaks of all three compounds we aimed to grow. The relatively poor signal-to-noise ratio of the diffraction peaks is due to the low film thickness and low crystallinity of the materials. We thus conclude that the films consist of higher domains of ferromagnetic $CoFe_2O_4$ and of lower domains of diamagnetic $BaTiO_3$ and ZnO, respectively.

dx.doi.org/10.1021/am201474t | ACS Appl. Mater. Interfaces 2012, 4, 40−43

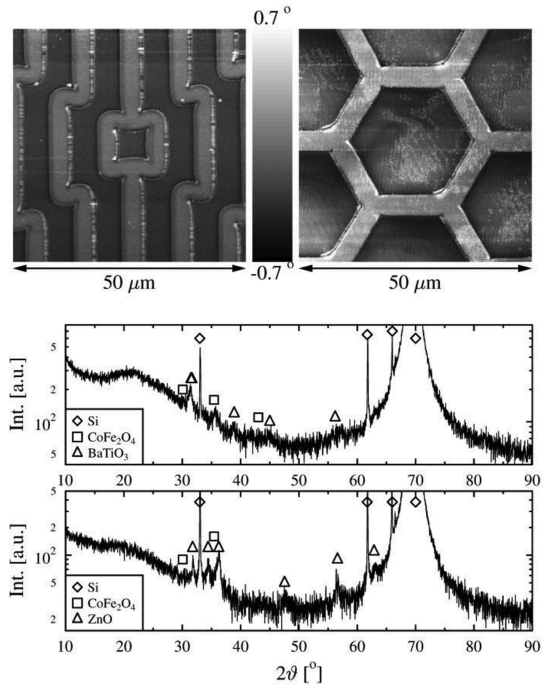

Figure 5. MFM images (top row) and X-ray diffractograms (middle and bottom) of two samples after heat treatment. The lift height for the MFM imaging was 70 and 50 nm, respectively. The phase of oscillation in the MFM images is relative, as the center of the range has been set to 0°, and thus no quantitative results can be obtained from the images. Top left, $CoFe_2O_4/BaTiO_3$; top right, $CoFe_2O_4/ZnO$; middle, $CoFe_2O_4/BaTiO_3$; bottom, $CoFe_2O_4/ZnO$.

4. CONCLUSIONS

Thin films of two functional oxides were laterally patterned over nearly 1 cm^2 by an uncomplicated soft lithographic method employing polymer- and sol–gel-based precursor solutions. X-ray diffraction shows that the films consist of two different compounds, while magnetic force microscopy proves that these compounds are laterally separated, the separation pattern being that of the initial soft-lithographic process. At the same time, the magnetic force microscopy, sensitive to a magnetic field of a material, shows that one physical property of the film, i.e., the remnant magnetization, could be patterned. It is to be expected that other physical properties, such as piezoelectricity, electrical conductivity, or remnant polarization, have been patterned simultaneously.

AUTHOR INFORMATION

Corresponding Author

*E-mail j.e.tenelshof@utwente.nl.

Present Address

†Bruker AXS, Dynamostraße 19, 68165 Mannheim, Germany

ACKNOWLEDGMENTS

Financial support of NWO-STW in the framework of the Vernieuwingsimpuls programme (VIDI) is acknowledged.

REFERENCES

(1) Xia, Y. N.; Whitesides, G. M. *Annu. Rev. Mater. Sci.* **1998**, *28*, 153–184.
(2) Martin, C. R.; Aksay, I. A. *J. Electroceram.* **2004**, *12*, 53–68.
(3) Masuda, Y. *J. Ceram. Soc. Jpn.* **2007**, *115*, 101–109.
(4) ten Elshof, J. E.; Khan, S. U.; Göbel, O. F. *J. Eur. Ceram. Soc.* **2010**, *30*, 1555–1577.
(5) Hampton, M. J.; Williams, S. S.; Zhou, Z.; Nunes, J.; Ko, D.-H.; Templeton, J. L.; Samulski, E. T.; DeSimone, J. M. *Adv. Mater.* **2008**, *20*, 2667–2673.
(6) Khan, S. U.; Göbel, O. F.; Blank, D. H. A.; ten Elshof, J. E. *ACS Appl. Mater. Interfaces* **2009**, *1*, 2250–2255.
(7) Kim, W. S.; Choi, D. G.; Bae, B. S. *Nanotechnology* **2006**, *17*, 3319–3324.
(8) Göbel, O. F.; Branfield, T. E.; Stawski, T. M.; Veldhuis, S. A.; Blank, D. H. A.; ten Elshof, J. E. *ACS Appl. Mater. Interfaces* **2010**, *2*, 2992–2994.
(9) Stawski, T. M.; Veldhuis, S. A.; Besselink, R.; Castricum, H. L.; Portale, G.; Blank, D. H. A.; ten Elshof, J. E. *J. Phys. Chem. C* **2011**, *115*, 20449–20459.
(10) Göbel, O. F.; Blank, D. H. A.; ten Elshof, J. E. *ACS Appl. Mater. Interfaces* **2010**, *2*, 536–543.
(11) Martin, C. R.; Aksay, I. A. *J. Phys. Chem. B* **2003**, *107*, 4261–4268.
(12) Verschuuren, M.; Van Sprang, H. In *Materials Research Society Symposium Proceedings*; Gigli, G., Ed.; Materials Research Society: Warrendale, PA, 2007; Vol. *1002E*, N03–05.